Biological tissues inspection based on the indices of polarimetric purity

Albert Van Eeckhout*[a], Angel Lizana*[a], Enric Garcia-Caurel[b], José J. Gil[c], Adrià Sansa[a], Carla Rodríguez[a], Irene Estévez[a], Emilio González[d,e], Juan C. Escalera[a], Ignacio Moreno[f], Juan Campos[a]
[a]Grup d'Òptica, Physics Department, Universitat Autònoma de Barcelona, Bellaterra, Spain; [b]LPICM, CNRS, École Polytechnique, Université Paris-Saclay, Palaiseau, France; [c]Laboratory of Polarimetry, ICE Universidad de Zaragoza, Zaragoza, Spain; [d]Departamento de Anatomía, Histología y Neurociencia, Universidad Autónoma de Madrid, Madrid, Spain; [e]Servicio de Anatomía Patológica, Hospital Universitario de Canarias, Santa Cruz de Tenerife, Spain; [f]Departamento de Ciencia de Materiales, Óptica y Tecnología Electrónica, Universidad Miguel Hernández de Elche, Elche, Spain

ABSTRACT

We highlight the interest of using the three Indices of Polarimetric Purity (IPPs) for the biological tissue inspection. These three indices are focused on the study of the depolarizing behaviour of the sample. The IPPs have been recently proposed in the literature and provide different and synthetized information than the commonly used indices, as depolarization index (P_Δ) or depolarization power (Δ). Compared with the standard polarimetric images of biological samples, IPPs enhance the contrast between different tissues of the sample and show differences between similar tissues which are not observed using the other standard techniques. Moreover, they present new information about the depolarization mechanisms produced in the tissues. In addition, the algorithm does not require advanced calculations (as in the case of polar decomposition), being the indices of polarimetric purity fast and easy to implement. We also propose a pseudo-coloured image which encodes the information of the different indices. These images allow us to improve the visualization of the samples and to have information about the different depolarization mechanisms. Pseudo-coloured images present the possibility to enhance the contrast of specific tissues by customizing the IPPs combination. The interest and power of the IPP approach are experimentally illustrated throughout the manuscript by comparing polarimetric images of different ex-vivo samples, obtained with the standard polarimetric methods and with the enhanced images based on the IPPs. Enhanced contrast and new information are experimentally obtained from the different IPP based images.

Keywords: Depolarization, Biological tissue, Mueller matrix, Polarimetry, Imaging.

1. INTRODUCTION

Light-matter interactions can modify the polarization of light. The study of this modifications provides information about the matter structure. These polarization-based techniques [1] are non-invasive methods which are used for a widespread number of applications [2-6]. Over the past few decades, polarimetric imaging has shown its potential in biomedical applications [7,8]. Leading to enhance the image contrast of the biological images [9-12], and also providing constitutive information of the biological structure [10-14]. As for instance, imaging polarimetry allows determining the degree of birefringence of different structures [15,16], describing scattering mechanisms in biological samples [17,18], determining the organization and density of fibers in tissues [15,19], etc. Nowadays, this polarimetric information obtained from biological samples are applied in medicine, for instance, to prevent eye disorders [20-22], to evaluate skin diseases [15,23,24] or to discriminate healthy and malignant areas for early cancer detection [25,27], among others.

Different approaches are developed to deal with the quantification and qualification of polarimetric interaction with biological structures. One group of polarimetric techniques are the so-called polarization gating [28-31]. Consisting of illuminating the sample using a known polarization (instead of the usual unpolarized light) and discriminating the sample response by analyzing a discrete polarization. The input illumination and the detected light polarization are chosen aiming the enhance of image contrast.

Another important group of polarimetric techniques is focused on measuring the Mueller Matrix (MM) [32-35] of samples. MMs are 4x4 matrices which determine how a polarization state (using the Stokes vector notification) is modified after an interaction with the sample. The 16 coefficients have the information about the polarimetric properties and can be used to enhance the contrast as well as to determine the biological structure of the sample. However, a combination of the coefficients leads to an accurate extraction of information. In fact, we have recently linked PG with MM, showing that PG is a discrete combination of MM coefficients [11].

Working with the different terms, besides being able to reproduce any PG combination, it is also possible to decompose the Mueller matrices into a series of well-known basic MMs[32-36]. Decomposition approaches are useful not only in terms of image contrast, but also to perform a physical interpretation of samples. However, decompositions are not able to extract all the information. In other words, each decomposition emphasizes some part of information (diattenuation, retardance or depolarization) and distort another part.

In the particular case of biological samples, some authors exhibit that the potential information is related to retardance[37,38], and depolarization[26,38,39]. The usual way to extract this information is to use the Lu-Chipman decomposition, which decomposes the MM into three basic MMs (pure diattenuator M_D, pure retarder M_R, depolarizer M_Δ). Diattenuator can be dismissed because it does not give relevant information in biological samples. Alternatively, from M_R, we can define different parameters with physical interpretation to characterize the retardance of the sample (eg global retardance, R, linear retardance, L_R, circular retardance, C_R, neutral and extraordinary axes orientation, etc. [33-35]). At analyzing the depolarization, it is restricted in observing the M_Δ coefficients, but it has a complementary artifact in order to satisfy the decomposition. Or at best, it is calculated the degree of polarimetric purity P_Δ, which measures the degree of depolarization, but without distinguishing the type of depolarization.

Recently, the so-called Indices of polarimetric purity (IPP) are described in the literature [40,41]. IPP is an alternative method to analyze the depolarizing behavior of a sample. The advantage of IPP in front of P_Δ is the classification of different types of depolarizer. Moreover, the classification of the depolarizers has a direct physical interpretation [42]. Nevertheless, the potential of this method is not exploited in biological camp.

In this proceeding, we highlight the interest of using this technique, not only to enhance the contrast, but also to obtain new information of the sample, which is hidden when the other methods are used. In fact, we perform two ex-vivo experiments which results are shown in this proceeding. This proceeding, also explains how to develop the method (mathematical background and instrumentation) to obtain significant benefits.

2. MATHEMATICAL BACKGROUND

This section summarizes the main mathematical foundations into the Mueller framework, defined previously by a number of authors [32-36, 40-45]. We focus on the mathematical expressions related to the depolarizing behaviours because they have improved the image contrast of the tissues analysed in section 4.

First, we separate the 4x4 MM into different physically known elements:

$$\hat{\boldsymbol{M}} = \boldsymbol{M} / m_{00} = \begin{pmatrix} 1 & \boldsymbol{D}^T \\ \boldsymbol{P} & \boldsymbol{m} \end{pmatrix} \tag{1}$$

where m_{00} is the mean intensity coefficient of **M**. **P** and **D** are called, respectively, the polarizance and diattenuation of **M** and are the absolute value of their corresponding vectors ($P \equiv |\mathbf{P}|$ and $D \equiv |\mathbf{D}|$).

Analogous to P and D, the degree of spherical purity, PS, which provides the depolarizing contribution of **m** is defined as,

$$P_S \equiv \frac{1}{\sqrt{3}} \sqrt{\sum_{i,j=1}^{3} m_{ij}^2}\,. \tag{2}$$

Combining the depolarization contributions we can provide a measurement of the depolarization defined by the depolarization index [41]

$$P_{\Delta} = \sqrt{(D^2 + P^2 + 3P_s^2)/3}. \quad (3)$$

In this expression, we are interested in P_Δ, and also in Ps which measure the contribution non-related to the diattenuation and polarizance, because they allow us to interpret different MM in terms of depolarization. Both parameters are restricted to the range $0 \leq P_\Delta \leq 1$ and $0 \leq P_S \leq 1$. Analysing different scenarios, the maximum value $P_\Delta = 1$ corresponds to a non-depolarizing media, $P_\Delta < 1$ is related to a depolarizer and the minimum value, and zero is associated with an ideal depolarizer (except m00, all the elements of the matrix are zero). A special case corresponds to a $P_S = 1$ which involves $P_\Delta = 1$ and corresponds to a pure (non-depolarizing) retarder MR.

Presented parameters provide a scheme of the matrices based on the extreme cases (ideal depolarizer or non-depolarizer), but real matrices are more complex and require further analysis. Mueller decompositions appear here as alternative techniques to bring this analysis. Decomposition method consists in decompose M into a combination or a sequence of matrix factors with a defined physical meaning. Examining biological samples, the most commonly used decomposition is the Lu-Chipman decomposition [32]. It decomposes the **M** as,

$$\boldsymbol{M} = \boldsymbol{M}_{\Delta}\boldsymbol{M}_{R}\boldsymbol{M}_{D}, \quad (4)$$

in which $\mathbf{M_\Delta}$ is a depolarizer, $\mathbf{M_R}$ is a retarder, and $\mathbf{M_D}$ is a diattenuator. Those three resulting matrices provide the depolarizing, retardance and diattenuation information about **M**. However, in the case of the depolarization, it is difficult to interpret the information because a polarizance vector, with no physical meaning, is added to satisfy the decomposition calculations.

The depolarization power (Δ),

$$\Delta = 1 - \frac{|tr(\boldsymbol{M}_{\Delta}) - 1|}{3}, \quad 0 \leq \Delta \leq 1, \quad (5)$$

which is quite equivalent to P_Δ, is the physical parameter commonly used to interpret this information, where Δ= 1 corresponds to an ideal depolarizer, and Δ=0 is associated with a non-depolarizing media.

A different approximation is the Cloude's decomposition [35]. It decomposes **M** into four pure Mueller matrices with different weights as

$$\boldsymbol{M} = m_{00}\sum_{i=1}^{4}\hat{\lambda}_i\hat{\boldsymbol{M}}_{Ji} \quad (6)$$

where $\mathbf{M_{Ji}}$ are the different pure Mueller matrices and λ_i are the eigenvalues of the associated covariance matrix **H** [34]. The eigenvalues are restricted to the range $0 \leq \hat{\lambda}_i \leq 1$ and are ordered as $\lambda_1 \geq \lambda_2 \geq \lambda_3 \geq \lambda_4 \geq 0$. The sum of all the eigenvalues is m_{00}, therefore the normalized eigenvalues are not completely independent and, at best, only three independent parameters can be obtained. Combining the eigenvalues we define three invariant and dimensionless indices of polarimetric purity (IPP)[35],

$$P_1 \equiv \hat{\lambda}_1 - \hat{\lambda}_2, \qquad P_2 \equiv \hat{\lambda}_1 + \hat{\lambda}_2 - 2\hat{\lambda}_3, \qquad P_3 \equiv \hat{\lambda}_1 + \hat{\lambda}_2 + \hat{\lambda}_3 - 3\hat{\lambda}_4, \quad (7)$$

which allows to describe and measure a different kind of depolarizers. IPPs values are restrained by the following inequality:

$$0 \leq P_1 \leq P_2 \leq P_3 \leq 1. \quad (8)$$

In the limiting cases, we observe pure matrices characterized by $P_1 = P_2 = P_3 = 1$ and ideal depolarizers defined by $P_1 = P_2 = P_3 = 0$. As expected, P_Δ is related to IPPs, and can be calculated as:

$$P_{\Delta}^2 = \frac{1}{3}\left(2P_1^2 + \frac{2}{3}P_2^2 + \frac{1}{3}P_3^2\right). \quad (9)$$

The advantage of the IPPs in front P_Δ is the classification of the depolarizers, as a recent manuscript has experimentally proved [42]. Moreover, IPPs can be represented into 3D space and constitute the so-called purity space, presented in Fig.1[35].

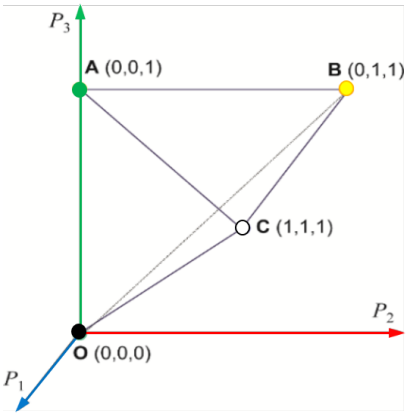

Figure 1 Representation of the purity space comprised by the indices of polarimetric purity P_1, P_2, P_3.

Observing the scheme we can easily classify the depolarizers into ideal depolarizers and pure matrices corresponding to O (0, 0, 0) (green spot) and C (1, 1, 1) (blue spot) respectively. But we are also able to measure the depolarization equivalent to the combination of two pure matrices (P_1), where the limiting case B (0, 1, 1) (orange spot) implies the same weight combination and measure the equivalent phenomena but with three matrices instead (P_2). A (0, 0, 1) is the specified case where the depolarizer can be described as a combination of three pure Mueller matrices with the same weights. The other cases, which corresponds to a point in the tetrahedron, is a depolarizer and can be studied using its associated P_1, P_2, and P_3.

3. EXPERIMENTAL SET-UP AND SAMPLES DESCRIPTION

In this section, we describe the optical setup implemented to measure the MM of the different biological samples, and we also describe the samples used for the ex-vivo experiments discussed in section 4.

The optical set-up implemented to measure the MMs of the biological samples is a complete Mueller Matrix based on Parallel Aligned Liquid Crystal (PA-LC) retarders (Fig.2). The optical architecture used is analogous to that provided in Ref. [46], but adapted to image polarimeter for biological inspection.

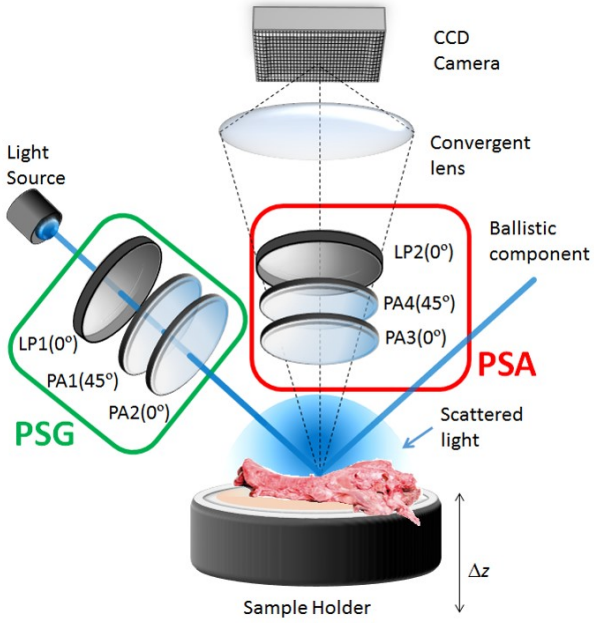

Figure 2 Optical scheme of the complete image polarimeter used to measure the MMs of biological samples.

First, the set-up is able to use different wavelength (625nm and 470nm). The penetration length into the samples depends on the wavelength [47] and it allows us to work with different penetration length. Illumination is generated by 4-Wavelength High-Power LED Source (Operated by DC4104 drivers distributed by Thorlabs) which is redirected by an optical fiber. The light pass throughout a Polarization State Generator (PSG) (marked with a green rectangle in Fig. 2) which is able to generate any state of polarization by adjusting the retardances of the two PA-LC panels as discussed in [46]. PSG is composed by a linear polarizer at 0º degrees to the laboratory vertical reference axis (Glan-Thompson prism based polarizer by CASIX), a first PA-LC panel (PA1), oriented at 45º to the laboratory vertical, and a second PA-LC panel oriented at 0º (PA2). The polarized light illuminates the sample with an incident angle of ~55º which holder can be mechanically displaced in the *z*-direction for imaging purposes. The scattered light is measured with a Polarization State Analyser (PSA) (marked with a red rectangle in Fig.2), which is constructed with the same optical elements than those in the PSG but with the inverse order. The linear polarizer at the PSA (LP2) is a dichroic sheet polarizer (by Meadowlark Optics) and for all the liquid crystal panels in the PSG and PSA, we used four Parallel Aligned Liquid Crystal Variable Retarders with Temperature Control (LVR–200–400-700-1LTSC by Meadowlark Optics). Finally, a convergent lens (TECHSPEC® High Resolution objective, distributed by Edmund Optics, with a focal length of 35 mm) images the sample on a CCD camera (Allied Vision Manta G-504B. It is a 5 Megapixel GigE Vision camera with the Sony ICX655 CCD sensor, with a 2452(H) × 2056(V) resolution and a cell size of 3.45 µm x 3.45 µm) with a spatial resolution of ~22 µm. PSG and PSA are covered by a plastic case specially designed and constructed by a 3D printer to robust the elements.

In terms of efficiency, at least 16 images of the region of interest (2.2 x 2.2 cm^2) are needed to obtain the Mueller Matrix of the sample by applying the inverse method [32-34]. This MM is achieved in few seconds (0.4 to 2.2 s), and the delay depends on the CCD exposure time.

Regarding the samples analysed in this work, we perform a polarimetric study of two different ex-vivo samples in order to highlight the improvement, in terms of image contrast, related to the use of the IPPs. The first sample is a trachea of a suckling lamb. The trachea is constructed by tracheal cartilages rings joined by a fibrous membrane called annular ligaments of the trachea. Tracheal cartilages are composed by hyaline cartilages which are made up of type II collagen and chondroitin sulphate. The fibrous membrane contains a large amount of collagen type I fibres and fibroblast cells. According to a pathologic analysis, the second sample, consists of an endocardial view of a dissected lamb heart, including endocardium-covered heart muscle and connective tissue rich in subvalvular apparatus.

4. BIOLOGICAL TISSUES IMAGE ENHANCEMENT BY USING THE INDICES OF POLARIMETRIC PURITY

In this section, we exhibit the interest of using the indices of polarimetric purity (IPPs) to study biological tissues. In particular, to perform this demonstration, we studied two samples described in section 3. First, we characterize a sample using the main polarimetric methods and we expose the image contrast enhancement, as well as, the new information obtained from the IPPs use, section 4.1. In order to not enlarge the manuscript, this discussion is carried out using only one sample (a region of a suckling lamb trachea, first sample in section 3) and in the follow section we present another ex-vivo case of interest.

4.1 Biological sample examination based on polarimetric methods

The trachea's MM of a suckling lamb was measured at 475 nm because we wanted to inspect the surface details of the sample, and large wavelength penetrates more [47]. The MM can be separated into 4 groups of information (intensity, diattenuation, depolarization, and retardance). First, Normal intensity image information is presented in the m_{00} and is represented in Figure 3 (a). This component describes the irradiance response of the sample against any polarization. In the case of diattenuation, many polarimetric studies about biological samples have shown that retardance and depolarization channels provide significant information [7-14, 17-24] while diattenuation channel can be depreciated. However, this significant information depends on the sample structure. The birefringent structure, as fiber collagen-based ones, presents higher response in retardance. In particular case, structures based on collagen fibers are very interesting, because we can describe the direction of the fibers from the retardance Mueller obtained from the Lu-chipman decomposition. But, not all the samples have this particularity, as in our case (Figure 3 (b)) in which the retardance response is not significant. Spatial disorganized structures composed of small scattering particles are more susceptible to depolarize the light.

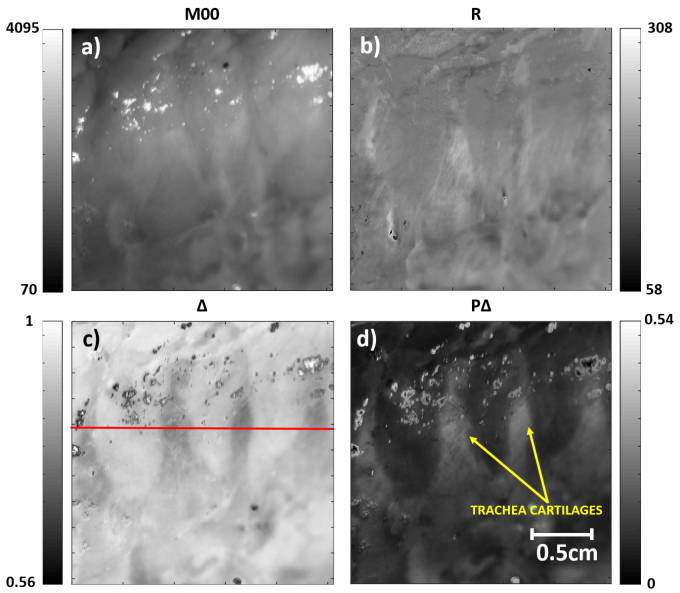

Figure 3 Polarimetric analysis of a trachea with tracheal cartilages rings (yellow arrow) (a) Regular intensity image (M_{00}); (b) retardance image R; (c) depolarization power Δ and (d) depolarization index P_{Δ}.

Our trachea has a similar structure to the last described and it depolarizes the incident light. But the light is depolarized in a different way depending on the structure of the different biological tissues. We measured two depolarizing indexes (depolarization power Δ and depolarizing index P_{Δ}) (Figure 3 (c) and (d)) which associate a number from 0 to 1 of the degree of depolarization. The two depolarizing methods are quite analogous because the information is similar, and they quantify the average output polarization. Comparing the results, we are able to distinguish trachea cartilages rings from the empty spaces. Rings are impossible to observe in intensity (M_{00}), and they are hard to observe in the total retardance (R). From the results, we can say that the light scattered over the rings better maintains the polarization than the others parts. Then, using this method we are able to quantify the depolarization process, but we are not able to qualify it. For that reason, we have calculated the IPP of this samples represented in Figure 4.

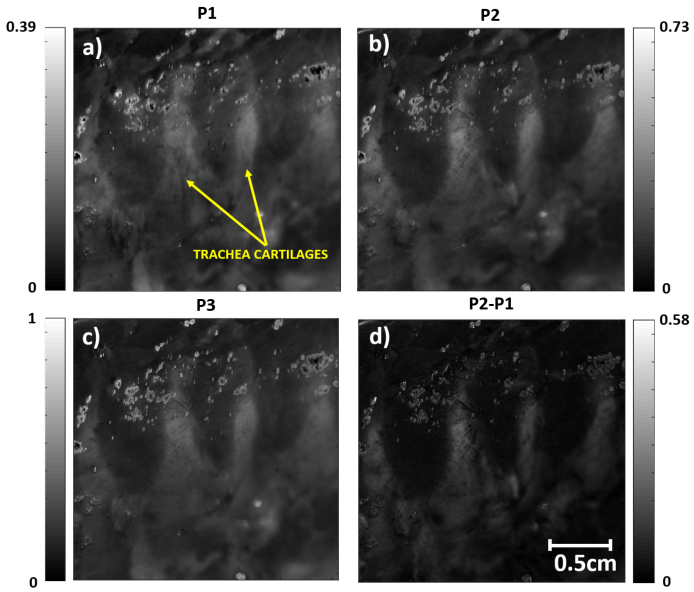

Figure 4 Polarimetric analysis of a trachea with tracheal cartilages rings (yellow arrow) (a) P_1; (b) P_2; (c) P_3 and (d) the difference between P_1 and P_2.

IPP responses are not much different to P_Δ, but these differences are really important. First, the information obtained from IPP and P_Δ are not analogous, because IPP describes the depolarization methods produced in the sample. Even though in the case that the images where identically, it would be a progress because we can determine the exact method of depolarization. Second, P_Δ is an average of the IPP calculated as Eq. (9), then, one of this terms has to enhance the contrast of some part of the sample with respect to P_Δ. In our case, IPP enhances the rings contrast. To illustrate it, we represented a cross-section (red line figure 3 (c)) of M_{00}, 1-Δ, P_Δ, P_2, and P_3. We represented 1-Δ instead of Δ because the information is the same, and 1-Δ is easy to compare in the graph. Also, we neglect the representation of some cross-section because the graph would be full of lines and now is easy to interpret. However, this neglected representation fulfills the idea that rings are invisible in MM, they can be seen in P_Δ and Δ, and IPP enhance the contrast of this rings making easy to see.

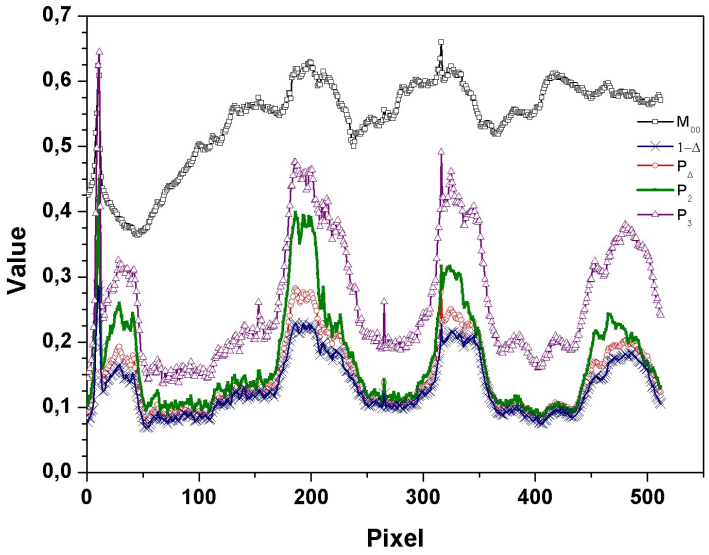

Figure 5 Graphical representation of trachea cross-section in the M_{00} (black □), 1-Δ (blue x), P_Δ (red ○), P_2 (green ▪) and P_3 (purple Δ) channels.

To numerically analyze this graphs, we have calculated the peak to valley (PV) and the visibility (V) of the central ring.

$$PV = \mathbf{I}_{\max} - \mathbf{I}_{\min}, \quad V = \frac{\mathbf{I}_{\max} - \mathbf{I}_{\min}}{\mathbf{I}_{\max} + \mathbf{I}_{\min}}. \tag{9}$$

In order to calculate PV and V, we rake the maximum value of the pick and the minimum value at the base of the pick. The results, represented in table 1, display a visibility of 0.48 for P_2 in front of 0.37 of P_Δ. It supposes a 30% of increment of the contrast with respect to the original method measuring this sample.

Table 1. Peak to valley and Visibility values for the different cross-sections of the sample polarization images.

	$\mathbf{M_{00}}$	**1-Δ**	$\mathbf{P_\Delta}$	$\mathbf{P_2}$	$\mathbf{P_3}$
PV	0.06	0.11	0.15	0.25	0.26
V	0.05	0.31	0.37	0.48	0.39

From data in table 1, we clearly observe the significant dependence of the contrast on the polarimetric channel, being P_2 the best channel to study the trachea.

Finally, we propose a pseudo-coloured image, associating a colour to each component, analogously to the three IPP representation in a purity space (Figure 1), but adding some weight in order to increase the importance of some component in front the others. The representation (Figure 6) follows the equation (10),

$$C_{pix}(x,y) = \alpha_1 P_1(x,y) + \alpha_2 P_2(x,y) + \alpha_3 P_3(x,y), \tag{10}$$

where P_1, P_2, and P_3 go from 0 to 1, and α_1, α_2, and α_3 are the respective weights which can be changed to enhance the contrast of different structures.

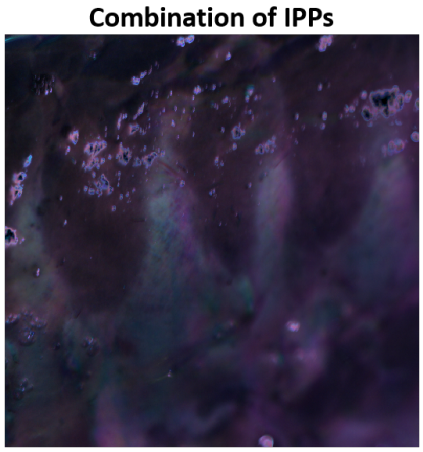

Figure 6 Pseudo-colored image obtained by using the Eq. (10) for $\alpha_1 = 3$, $\alpha_2 = 1$ and $\alpha_3 = 1$ of a trachea with tracheal cartilages rings.

The pseudo-coloured picture is obtained of the combination proposed in the equation 10 with the weights $\alpha_1=2$, $\alpha_2=1$ and $\alpha_3=1$. The pseudo-coloured method allows representing the information of the different ways to depolarize the light produced in the biological structure in a single image by associating colours to different depolarizing processes. We can observe that the ring has different colours in the extremes than in the center which is associated with the thickness. The different thickness is clearly represented by two different colours (near to green, and near to purple) and they are related to the depolarization processes.

4.2 *Ex-vivo* case of interest

In section 4.1 we have qualitative demonstrated the enhancement in contrast provided by the IPP channels. But, this is only one experiment. In this section 4.2, we will show the interest of using IPP, demonstrating that the enhancement is not a particular case of some samples and it is recurrent.

We measured the second sample (Figure 7), a ROI into a lamb heart, using a 625nm wavelength to penetrate more [47]. Analogous with the trachea, we have applied the same methods, but we represented only the regular intensity image (M_{00} in Fig. 7 (a)), the retardance (R in Fig. 7 (b)), the depolarization index (P_Δ) and two combinations of IPP (Fig. 7 (d) and (e)). In Fig. 7 (d) we used Eq.(9) and the weights are $\alpha1 = 3$, $\alpha2 = 1$ and $\alpha3 = 1$. But to develop the las IPP combination we have used another equation.

$$C_{pix}(x,y) = \alpha_1 \left[\frac{P_1(x,y) + P_2(x,y) + P_3(x,y)}{3} \right] + \alpha_2 \left[\frac{P_2(x,y) + P_3(x,y)}{2} \right] + \alpha_3 P_3(x,y), \tag{11}$$

The possible combination of the channels is not unique, and in this manuscript, we only show representative options. However, note that all the terms in the equations go from 0 to 1. We choose a different equation, with different weights, $\alpha_1 = 1$, $\alpha_2 = 1$ and $\alpha_3 = 1$, to demonstrate the possibility of emphasizing different biological structures.

Analyzing the regular intensity image (M_{00}) we observe some cardiac tissue muscles, heart valves, and cavities but with a non-uniform light. This is a recurrent issue in biological sampling, and it is produced because that the sample is not flat (is a 3D volume) and then, in some angles appears a direct reflection, while in other angles, the light measured is only

the scattered. This differences in illumination do not appear in the polarimetric channels because they are independent of the light intensity. One of this channels is the retardance R. We observe spatial variations in birefringent response, but it is difficult to associate the response to a concrete biological structure. Unlike R, we see with better contrast than M_{00} some heart structures as heart valves and muscles in depolarization index image P_{Δ}. Finally, pseudo-coloured compositions have really enhanced contrast and heart valves and cavities are clearly observable and highly contrasted. Moreover, heart blood capillaries are now visible in Fig. 7 (d) which demonstrate the capability of extracting new information of IPP method. We want to emphasize that IPP not only are able to enhance the contrast but also can provide new unique information.

We present two different pseudo-coloured images, and comparing them we observe Fig. 7 (d) is focused on increasing the contrast of heart blood capillaries while in Fig. 7 (e) these capillaries are invisible. The absence of the capillaries is a reasonable lose because in Fig 7 (e) we wanted to put the attention into enhancing the connective rich insertion site contrast.

Two last pseudo-coloured examples denote the versatility of the technique and the possibility in emphasizing different structures.

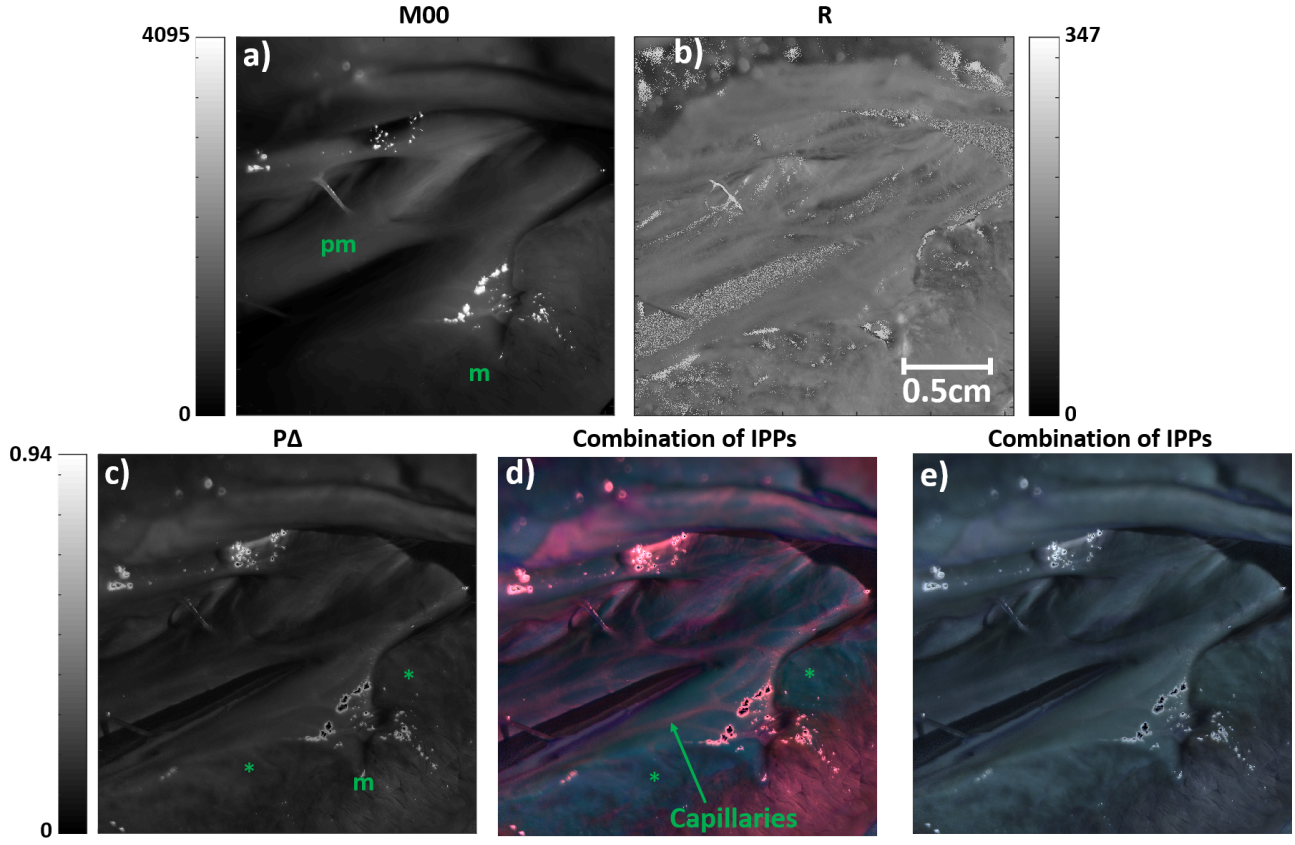

Figura 7 Polarimetric analysis of an endocardial view of the ventricular cavity with solid myocardium (m) and papillary muscles (pm) including their connective rich insertion site, "*". (a) Regular intensity image (M_{00}); (b) retardance image R; (c) depolarization index P_{Δ}; (d) pseudo-colored image obtained by using the Eq. (10) for $\alpha_1 = 3$, $\alpha_2 = 1$ and $\alpha_3 = 1$ and (e) pseudo-colored image of obtained by using the Eq. (10) for $\alpha_1 = 1$, $\alpha_2 = 1$ and $\alpha_3 = 1$.

5. CONCLUSION

IPP is a polarimetric method recently proposed in the literature, which sinthethize the depolarizing properties of samples. We request the use of the IPP for the biological tissues examination. These indices provide an enhanced contrast and new

information respect to standard polarimetric images. They also allow developing a physical interpretation related to the depolarizing mechanisms of the structure as demonstrated in [42].

We also propose a pseudo-coloured image which encodes the information of the different indices and improve the visualization. The potential of the IPP approach is experimentally illustrated by comparing polarimetric images of different ex-vivo samples, obtained with the standard polarimetric methods and by presenting the enhanced images based on the IPPs. We provide two ex-vivo examples, but we observed the advantages in larger number samples which are not included in this work to prevent the proceeding to be excessively long and redundant.

REFERENCES

[1] R. M. A. Azzam, N. M. Bashara, [Ellipsometry and Polarized Light], North-Holland Publishing Company, Amsterdam, (1977).

[2] J. Hough, Astron. "Polarimetry: a powerful diagnostic tool in astronomy," Geophys 47, 3.31-3.35 (2006).

[3] N. Uribe-Patarroyo, A. Alvarez-Herrero, R. L. Heredero, J. C. del Toro, A. C. López, V. Domingo, J. L. Gasent, L. Jochum, V. Martínez, "You have full-text access to this contentIMaX: a polarimeter based on Liquid Crystal Variable Retarders for an aerospace mission," Phys. Status Solidi C 5, 1041-1045 (2008).

[4] J. S. Tyo, D. L. Goldstein, D. B. Chenault, J. A. Shaw, "Review of passive imaging polarimetry for remote sensing applications," Appl. Optics 45, 5453-5469 (2006).

[5] D. M. Shinki, M. T. Ivanov, J. S. Post, S. Vagle, J. T. Cullen, D. K. Hore, "An auto-calibrating Stokes polarimeter for materials characterization," Appl. Optics 51, 4113-4119 (2012).

[6] A. Lizana, M. Foldyna, M. Stchakovsky, B. Georges, N. David, E. GarciaCaurel, "Enhanced sensitivity to dielectric function and thickness of absorbing thin film by combining total internal reflection ellipsometry with standard ellipsometry and reflectometry," J. Phys. D Appl. Phys. 46, 105501 (2013).

[7] T. Novikova, I. Meglinski, J. C. Ramella-Roman, V. V. Tuchin, "Special section on polarized light for biomedical applications," J. Biomed. Opt. 21, 071001 (2016).

[8] V. V. Tuchin, "Polarized light interaction with tissues," J. Biomed. Opt. 21, 071114 (2016).

[9] J. L. Arce-Diego, F. Fanjul-Vélez, D. Samperio-García, D. Pereda-Cubián, "Mueller coherency matrix method for contrast image in tissue polarimetry," Proc. SPIE 6627, 66271T (2007).

[10] J. Qi, D. S. Elson, "A high definition Mueller polarimetric endoscope for tissue characterization," Sci. Rep. 6, 25953 (2016).

[11] A. Lizana, A. Van Eeckhout, K. Adamczyk, C. Rodríguez, J. C. Escalera, E. Garcia-Caurel, I. Moreno, J. Campos, "Polarization gating based on Mueller matrices," J. Biomed. Opt. 22, 056004 (2017).

[12] J. Qi, D. S. Elson, "Mueller polarimetric imaging for surgical and diagnostic applications: a review," J. Biophotonics 10, 950 (2017).

[13] H. He, C. He, J. Chang, D. Lv, J. Wu, C. Duan, Q. Zhou, N. Zeng, Y. He, H. Ma, "Monitoring microstructural variations of fresh skeletal muscle tissues by Mueller matrix imaging," J. Biophotonics, 10, 664-673 (2017).

[14] Y. A. Ushenko, "Investigation of formation and interrelations of polarization singular structure and Mueller-matrix images of biological tissues and diagnostics of their cancer changes," J. Biomed. Opt. 16, 066006 (2011).

[15] T. Yasui, Y. Tohno, T. Araki, "Characterization of collagen orientation in human dermis by two-dimensional second-harmonic-generation polarimetry," J. Biomed. Opt. 9, 259-264 (2004).

[16] M. C. Pierce, J. Strasswimmer, B. Hyle Park, B. Cense, J. F. De Boer, "Birefringence measurements in human skin using polarization-sensitive optical coherence tomography," J. Biomed. Opt. 9, 287-291 (2004).

[17] V. V. Tuchin, Tissue Optics: Light Scattering Methods and Instruments for Medical Diagnosis, SPIE Press, Bellingham (2007).

[18] N. Ghosh, M. F. Wood, I. Vitkin, "Mueller matrix decomposition for extraction of individual polarization parameters from complex turbid media exhibiting multiple scattering, optical activity, and linear birefringence," J. Biomed. Opt. 3, 044036 (2008).

[19] K. Komatsu, L. Mosekilde, A. Viidik, M. Chiba, "Polarized light microscopic analyses of collagen fibers in the rat incisor periodontal ligament in relation to areas, regions, and ages," Anat. Rec. 268, 381-387 (2002).

[20] K.M. Twietmeyer, R.A. Chipman, A.E. Elsner, Y. Zhao, and D. VanNasdale, "Mueller matrix retinal imager with optimized polarization conditions," Opt. Express 16, p. 21339–21354 (2008).

[21] J.M. Bueno, “Measurement of parameters of polarization in the living human eye using image polarimetry,” Vision Research 40, p. 3791–3799 (2000).
[22] R. Rawer, W. Stork, and K.D. Müller-Glaser, “Polarimetric methods for measurement of intra ocular glucose concentration,” Biomed. Tech. 47, p. 186-8 (2002).
[23] L. Graham, Y. Yitzhaky, and I. Abdulhalim, “Classification of skin moles from optical spectropolarimetric images: a pilot study,” J. Biomed. Opt. 18, p.111403 (2013).
[24] Y. Yitzhaky, L. Graham, and I. Abdulhalim, “Analysis of skin moles from optical spectropolarimetric images,” Proc. of SPIE 8856, p. 88562J-1 (2013).
[25] T. Novikova, A. Pierangelo, A. De Martino, A. Benali, and P. Validire, “Polarimetric imaging for cancer diagnosis and staging,” Opt. Phot. News 23, p. 26-33 (2012).
[26] A. Pierangelo, A. Nazac, A. Benali, P. Validire, H. Cohen, T. Novikova, B.H. Ibrahim, S. Manhas, C. Fallet, M.R. Antonelli, and A. De Martino, “Polarimetric imaging of uterine cervix: a case study,” Opt. Express 21, p. 14120 –14130 (2013).
[27] E. Du, H. He, N. Zeng, M. Sun, Y. Guo, J. Wu, S. Liu and H. Ma, “Mueller matrix polarimetry for differentiating characteristic features of cancerous tissues,” J. Biomed. Opt. 19, 076013 (2014).
[28] P. Shukla, and A. Pradhan, “Polarization-gated imaging in tissue phantoms: effect of size distribution,” Appl. Opt. 48, p. 6099-6104 (2009).
[29] B. Kunnen, C. Macdonald, A. Doronin, S. Jacques, M. Eccles, and I. Meglinski, “Application of circularly polarized light for non-invasive diagnosis of cancerous tissues and turbid tissue-like scattering media,” J. Biophotonics 8, p. 317-323 (2015).
[30] Ch.W. Sun, Ch.Y. Wang, C.C. Yang, Y.W. Kiang, I.J. Hsu, and Ch.W. Lin, “Polarization gating in ultrafast-optics imaging of skeletal muscle tissues,” Opt. Lett. 26, p. 432-434 (2001).
[31] S. Sridhar, and A. Da Silva, “Enhanced contrast and depth resolution in polarization imaging using elliptically polarized light,” J. Biomed. Opt. 21, 071107 (2016).
[32] D. Goldstein, [Polarized Light], 2nd ed., Marcel Dekker, New York (2003).
[33] E. Garcia-Caurel, R. Ossikovski, M. Foldyna, A. Pierangelo, B. Drévillon, A. De Martino, [Advanced Mueller Ellipsometry Instrumentation and Data Analysis] Eds: M. Losurdo, K. Hingerls, Springer-Varlag, Berlin (2013).
[34] R. A. Chipman, [Polarimetry: Handbook of Optics], 2nd ed. McGrawHill, New York, (1995).
[35] J. J. Gil, R. Ossikovski, [Polarized Light and the Mueller Matrix Approach] CRC Press, Boca Raton, FL (2016).
[36] R. Ossikovski, “Differential and product Mueller matrix decompositions: a formal comparison,” Opt. Lett. 37, 220 (2012).
[37] C. He, H. He, J. Chang, Y. Dong, S. Liu, N. Zeng, Y. He, H. Ma, “Characterizing microstructures of cancerous tissues using multispectral transformed Mueller matrix polarization parameters,” Biomed. Opt. Express 6, 2934 (2015).
[38] M. K. Swami, S. Manhas, P. Buddhiwant, N. Ghosh, A. Uppal, P. K. Gupta, “Polar decomposition of 3×3 Mueller matrix: a tool for quantitative tissue polarimetry,” Opt. Express 14, 9324 (2006).
[39] A. Pierangelo, A. Benali, M. R. Antonelli, T. Novikova, P. Validire, B. Gayet, A. De Martino, “Ex-vivo characterization of human colon cancer by Mueller polarimetric imaging,” Opt. Express 19, 1582-1593 (2011).
[40] J. J. Gil, J. M. Correas, P. A. Melero, C. Ferreira, “Generalized polarization algebra,” Monog. Sem. Mat. G. Galdeano 31, 161 (2004).
[41] J. J. Gil, “Invariant quantities of a Mueller matrix under rotation and retarder transformations,” J. Opt. Soc. Am. A 33, 52 (2016).
[42] A. Van Eeckhout, A. Lizana, E. Garcia-Caurel, J. J. Gil, R. Ossikovski, J. Campos, “Synthesis and characterization of depolarizing samples based on the indices of polarimetric purity,” Opt. Lett. 42, 4155 (2017).
[43] J. J. Gil, E. Bernabéu, “Obtainment of the polarizing and retardation parameters of a non-depolarizing optical system from the polar decomposition of its Mueller matrix,” Opt. Acta 33, 185 (1986).
[44] I. San Jose, “Invariant indices of polarimetric purity: generalized indices of purity for n× n covariance matrices,” J. J. Gil, Opt. Commun. 284, 38 (2011).
[45] J. J. Gil, “Components of purity of a Mueller matrix,” J. Opt. Soc. Am. A 28, 1578 (2011).
[46] A. Peinado, A. Lizana, J. Vidal, C. Iemmi, and J. Campos, “Optimization and performance criteria of a Stokes polarimeter based on two variable retarders,” Opt. Express 18, 9815-9830 (2010).
[47] F. H. Mustafa, M. S. Jaafar, “Comparison of wavelength-dependent penetration depths of lasers in different types of skin in photodynamic therapy,” Indian J. Phys. 87, 203 (2013).